King's Research Portal

Document Version
Peer reviewed version

[Link to publication record in King's Research Portal](#)

Download date: 27. Dec. 2024

Experimental results of a YBCO bulk superconducting undulator magnetic optimisation*

Marco Calvi,† Alexandre Arsenault, Xiaoyang Liang, and Thomas Schmidt
Photon Science Division, Paul Scherrer Institute, Villigen PSI, Switzerland

Anthony R. Dennis and John H. Durrell
*Department of Engineering, University of Cambridge,
Trumpington Street, Cambridge, United Kingdom*

Carlos Gafa, Andrew Sammut, and Nicholas Sammut
University of Malta, Msida, Malta, MSD2080

Mark D. Ainslie
Department of Engineering, King's College London, Strand, London WC2R 2LS, United Kingdom

Ryota Kinjo
Osaka Institute of Technology, 5 Chome-16-1 Omiya, Asahi Ward, Osaka, 535-8585, Japon

Kai Zhang
Zhangjiang Laboratory, Shanghai, 201210, China

Sebastian Hellmann
Victoria University of Wellington, PO Box 600, Wellington 6140, New Zealand
(Dated: September 3, 2024)

The magnetic field optimisation of RE-Ba-Cu-O (REBCO, RE = Rare Earth) bulk superconducting undulators is a fundamental step towards their implementation in an accelerator driven photon source, like a synchrotron or a free electron laser. In this article we propose a sorting algorithm to reduce the undulator's phase error based on the reconstruction of the trapped current inside the bulks of a staggered array undulator. The results obtained with a YBCO short prototype field cooled down to $10\,\mathrm{K}$ in a $10\,\mathrm{T}$ magnetic field are reported. Finally, its performance is critically discussed in light of the 2D magnetic field map of its individual components, obtained at $\mathrm{LN_2}$ after the magnetization tests.

I. INTRODUCTION

Modern accelerator based photon sources, such as synchrotrons and free electron lasers (FELs), are based on undulator radiation. To improve their brightness and/or to reduce their costs, alternatives to the existing permanent magnet undulator (PMUs) [1–3] technology are required. Low temperature superconductors like NbTi [4–6] and more recently $\mathrm{Nb_3Sn}$ [7] have been employed to wind undulator coils with shorter period and higher magnetic fields. High temperature superconductors (HTS) in the form of tapes [8, 9] and bulks [10–12] promise to be the next step in increasing the performance of undulators. The increased operating temperature of HTS may also offer the prospect of reduced running costs. The present authors have concentrated their research effort on RE-Ba-Cu-O (REBCO, RE = Rare Earth) bulk [13, 14] staggered arrays in both planar [15, 16] and helical undulator [17] configurations. The first approach is more

suitable for synchrotrons [18], while the second one could be used in FELs [19, 20].

Manufacturing variation in the properties of bulk superconductors, in particular the local critical current density J_c, has to be compensated by an optimisation strategy in undulator applications, as is the case for PMUs. To permit this, the bulks are stacked one after the other in our design, and their order can be changed to improve the periodicity of the on-axis magnetic field profile (i.e. the RMS phase error [21]). In this work, an optimisation algorithm is proposed and its efficiency is demonstrated on a YBCO based short prototype undulator specially prepared for this purpose. The characterisation of the short undulator prototype was performed in the $12\,\mathrm{T}$ solenoid facility available at the Royce Institute at the University of Cambridge.

II. THE SORTING ALGORITHM

To develop an algorithm to find the optimum location of a set of bulks in a staggered array undulator, it is first required to identify which attributes are to be used for the optimisation process. The inverse analysis proposed
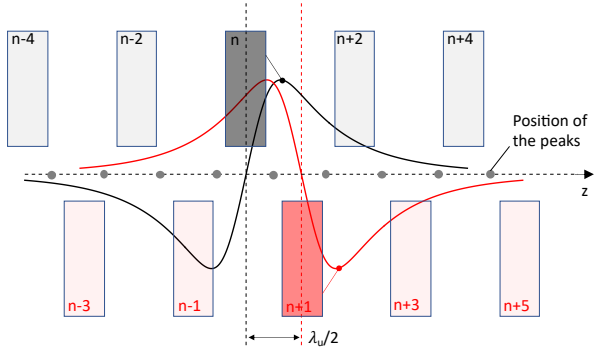
---

† marco.calvi@psi.ch

FIG. 1. The scheme of an infinite staggered array undulator where the magnetic field, $\psi(z)$, generated by the n-th bulk (in black) and the $n+1$-th bulk (in red) are plotted. The position of the undulator peak field is marked with gray solid circles.
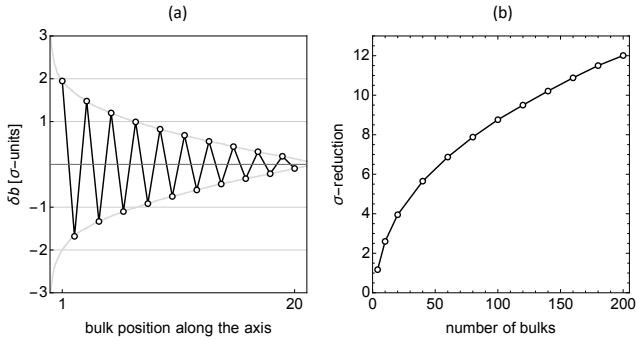

FIG. 2. On the left (a), the proposed spatial distribution of δb_n is shown, which reduces the magnetic field errors σ_B in the staggered array undulator. For reference, the optimum distribution for a large number of bulks (asymptotic), starting from a Normal distribution of b_n, is shown in gray. In black, 20 bulks are overlapped to schematically illustrate the optimisation algorithm. In this distribution, the average value is set at the right edge of the array, though other configurations are also possible. On the right (b), the reduction of the error using this spatial distribution is depicted, where the δb_n values also follow a Normal distribution.

in [22] will be used for this purpose. Kinjo's approach estimates the contribution of each n-bulk to the on-axis magnetic field profile $B(z)$ as a positive coefficient which multiplies the critical current density: $p_n J_c(B, T)$. The model assumes that the bulks have homogeneous properties, i.e. J_c depends only on the local magnetic field and temperature but not directly on the coordinates. Under these assumptions the field profile of an infinitely long undulator (see Fig. 1) can be well approximated by the following analytical expression,

$$B(z) = \sum_n (-1)^n b_n \psi(z - n\lambda_u/2), \tag{1}$$

where λ_u is the period length of the undulator, $\psi(-z) = -\psi(z)$ is the nominal magnetic field profile generated by a single bulk, and b_n its amplitude variation which is

intimately related to p_n, even if not identical, since the complexity of the bulk magnetization is neglected and thus no variation in penetration depth is taken into account. In other words, the amplitude of the n-th pole can be written as

$$B_n = \left| \sum_k (-1)^k b_k \psi[\lambda_u/4 + (n-k)\lambda_u/2] \right|. \tag{2}$$

To simplify the notation it is convenient to define

$$\psi_k \equiv \psi[\lambda_u(2k-1)/4]. \tag{3}$$

Using this definition results in (2) becoming,

$$B_n = \left| \sum_{k=1} (-1)^k (b_{n+k} + b_{n-k+1}) \psi_k \right|. \tag{4}$$

The aim of the optimisation process is to reduce the standard deviation of B_n

$$\sigma_B^2 = \frac{1}{N} \sum_{n=1}^N (B_n - \langle B_n \rangle)^2 \tag{5}$$

which can be written as a function of b_k using (4). To simplify the expression and to draw some preliminary conclusions we are accounting only for the nearest neighbours, so we may write the above formula as

$$\sigma_B^2/\psi_1^2 = \frac{1}{N} \sum_{n=1}^N (b_n + b_{n+1} - 2\langle b_n \rangle)^2 \tag{6}$$

and subtracting the average value ($\delta b_n = b_n - \langle b_n \rangle$) it further simplifies to the expression below

$$\sigma_B^2/\psi_1^2 = \frac{1}{N} \sum_{n=1}^N (\delta b_n + \delta b_{n+1})^2, \tag{7}$$

where the standard deviation σ_b can be highlighted and compared to the final one of σ_B,

$$\sigma_B^2/\psi_1^2 = 2\sigma_b^2 + \frac{2}{N} \sum_{n=1}^N \delta b_n \delta b_{n+1}. \tag{8}$$

Recognising that the last term above is an average value, it can be written in the following compact form,

$$\sigma_B^2/\psi_1^2 = 2\sigma_b^2 + 2\langle \delta b_n \delta b_{n+1} \rangle, \tag{9}$$

and diving by $\langle B \rangle^2$ both sides, we obtain the final formula which does not depend any longer on ψ_1,

$$\sigma_B^2/\langle B \rangle^2 = \tfrac{1}{2} \sigma_b^2/\langle b \rangle^2 + \tfrac{1}{2} \langle \delta b_n \delta b_{n+1} \rangle/\langle b \rangle^2. \tag{10}$$

If the spatial distribution of b_n is completely random, the second term is close to zero, and the relative standard deviation of B is $\sigma_b/\langle b \rangle/\sqrt{2}$. The coefficient $\sqrt{2}$ indicates that the relative error in one pole is reduced compared
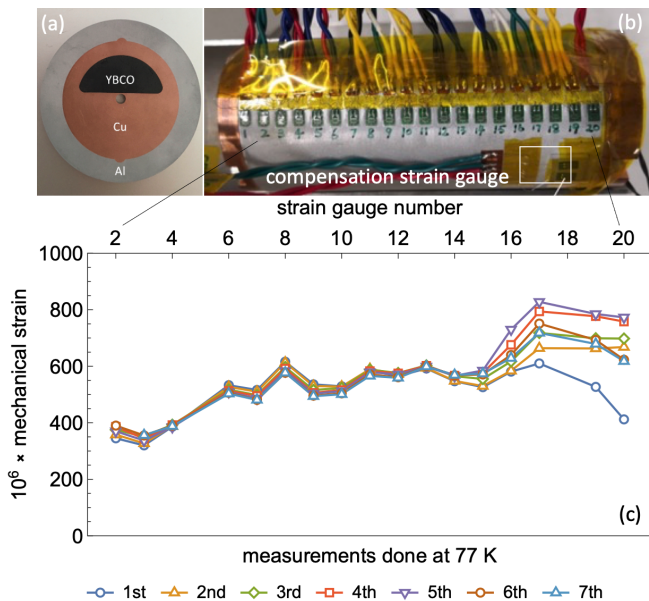
FIG. 3. On the top (a) the cross section of the sample where the Al cylinder, the Cu disk and YBCO bulk are highlighted and (b) the short undulator prototype after mounting strain gauges; on the bottom, (c) the measured mechanical hoop strains along the length of the aluminium shell after each thermal cycle training at 77 K.

to that of a single bulk because, in this approximation, one pole is the sum of two bulks, thus statistically mitigating the error. More remarkably, a specific choice of b_n spatial distribution can either increase or decrease the final sigma. If the sign of δb_n oscillates as $(-1)^n$, then the spread generated by the bulk production is reduced thanks to the second term (the average term) because it is negative. In Fig. 2a, an oscillating spatial distributions of δb_n is proposed which positions the average value in one of the extremes of the array. In Fig. 2b, the numerical solution of the equation (10) is calculated which gives the estimation of the reduction of $\sigma_B/\langle B\rangle$ as a function of the number of bulks, up to 200 units which is the target for the future full scale prototype. The following short prototype, prepared for this experiment, consists of 20 bulks and the above distribution was used for its optimisation where the model predicts an average spread reduction of 4.0±1.1.

III. SHORT PROTOTYPE UNDULATOR PREPARATION

The short prototype undulator was prepared following almost the same approach presented in [16]: a magnetic gap of 4 mm and a period length of 10 mm. The YBCO bulks fabricated by ATZ GmbH were ground to 4 mm thickness with a precision of 5 µm and wire eroded with electrical discharge machining (EDM) to their final half moon shape with the same accuracy. This precision is

required for shrink fitting them into their oxygen free copper sleeves which are only 10 µm smaller. The sleeves have to be heated up to 200 °C to allow the bulk to be inserted. 1.0 mm thick CoFe poles are added in between the bulks to enhance the undulator field strength. In contrast to [16], the stack of poles and bulks fits into an aluminum hollow cylinder (later referred simply as the Al-shell) which guarantees the relative position accuracy of the bulks within the array and provides additional pre-stress to the YBCO after the cool-down. As demonstrated in [16] it is not essential to shrink-fit the Al-shell onto the copper disks. Consequently the Al-shell was designed based on transition fitting (for easy assembly, the long shell is heated up to 200°C). To determine the contact status between the Al-shell and copper disks after cool-down, we mounted 20 strain gauges along the shell of one spare short prototype and two gauges on a small stress-free aluminium block for thermal compensation, as shown in Fig.3-top. Fig.3-bottom summarizes the recorded mechanical strains after each thermal cycle at 77 K. All strain data are positive, because the Al-shell experiences tensile hoop stress along the axial length and the copper disks are well compressed at 77 K. This demonstrates that the transition fit between the long aluminium shell and copper disks is a feasible solution in terms of mechanical stability. It should be pointed out that the right end of the Al-shell is connected to a thick copper plate and experiences large tensile mechanical strains combined with training effects. This is believed to be caused by the fact that the copper plate shrinks less than the aluminium shell and partially retards its shrinkage.

After assembly, the short undulator prototype was connected to the vertical magnetic field measurement system and installed in a variable temperature insert in the 12 T superconducting solenoid in the Cambridge Royce Institute. The undulator is cooled directly by flowing helium gas and its working temperature is controlled by a heater wrapped on the outer aluminium shell. A 3 mm-diameter x3yz-probe supported by a meter-long carbon fibre reinforced plastic (CFRP) tube and controlled by a motorized linear stage outside the cryostat, is employed to characterise the on-axis magnetic field in three orthogonal directions. The undulator field B_y is measured at three different y-positions, with one on-axis and the other two off-axis of ±0.1 mm. For other details regarding the experimental setup, please refer to [15].

IV. EXPERIMENTAL RESULTS

The prototype was field-cooled magnetised (FCM) first at 8 T, and the undulator magnetic field profile was recorded during the ramp-down of the external solenoidal field to monitor its evolution. This lower initial field-cooling value was selected prudently to avoid damaging the prototype before acquiring preliminary data. After reaching zero external field, the undulator was sub-cooled
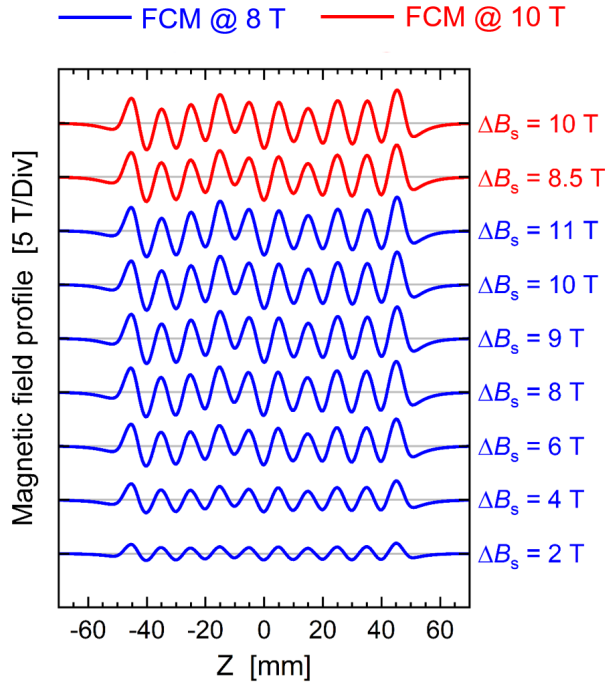
FIG. 4. The on-axis magnetic field measurement results before sorting. The blue curves result from the field-cooling magnetisation at 8 T while the red at 10 T.
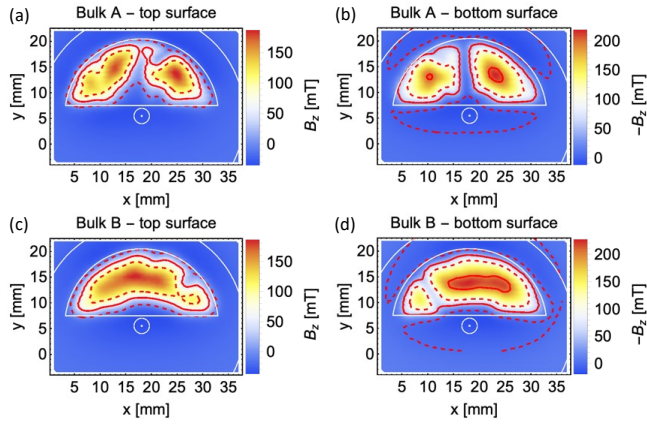

FIG. 5. The 2D maps of the magnetic field component (B_z) perpendicular to the bulk surface of two Cu-YBCO disks measured at LN_2. The left plots (a) and (c) show the maps of their top surfaces, while the right plots (b) and (d) display the maps of their bottom surfaces. These results are representative of this production batch, though not all data is presented here.

to 7 K to continue the charging process the following day without significant field loss. The sample was then warmed to the nominal 10 K, and the solenoid was driven below zero, ending the experiment at $B_s = -3$ T. After warming the undulator to 100 K, a second FCM was performed at the nominal magnetic field value of 10 T. The full set of data is reported in Fig. 4, where the un-
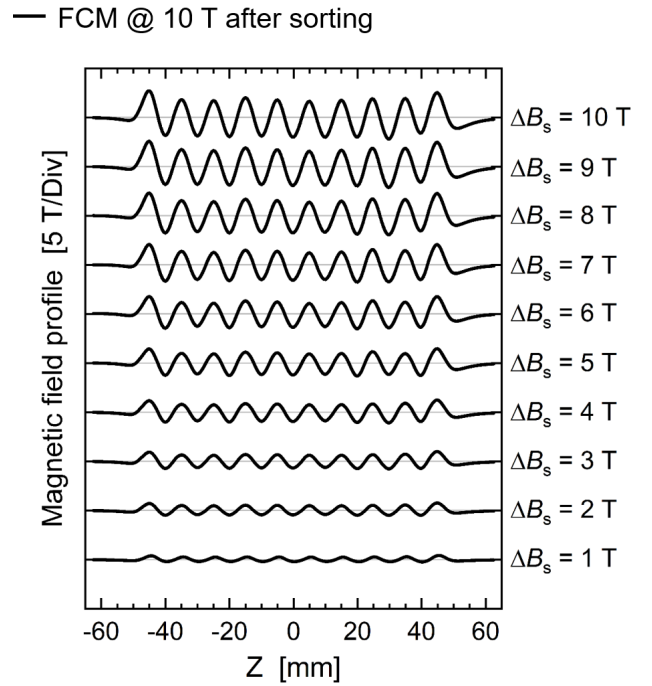

FIG. 6. The on-axis magnetic field measurement results after sorting at different ΔB_s.
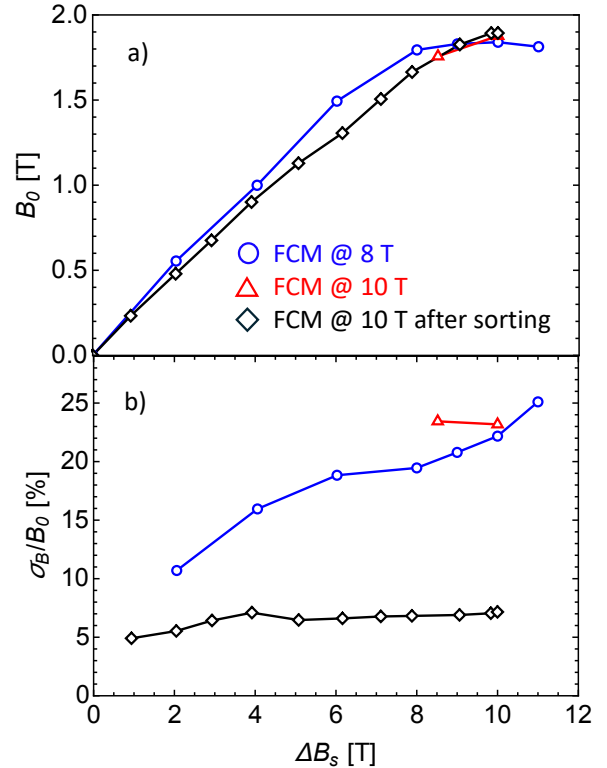

FIG. 7. Top, (a) the summary of the undulator magnetic field profile and bottom (b) its spread as a function of the solenoidal field swap, ΔB_s. The reduction of σ_B between the two final states ($\Delta B_s = 10$ T) is 3.2.

dulator magnetic field profiles are shown, with the 8 T FCM profile in blue and the 10 T FCM profile in red. Due to technical problems, data from the second run are available only at two points along the charging ramp, $\Delta B_s = 8.5\,\mathrm{T}$ and $\Delta B_s = 10\,\mathrm{T}$. It is noticeable that the prototype assembly exhibits highly uneven bulk behavior. Consequently, the prototype was warmed up, disassembled and its individual disks were magnetised separately at LN_2 to investigate the issue. A representative example of these 2D field maps of individual bulks is presented in Fig. 5, showing clear damage that qualitatively explains the highly inhomogeneous magnetic field profiles.

The final magnetic field profile recorded during the second run ($\Delta B_s = 10\,\mathrm{T}$) was used for a quantitative analysis of the contribution of individual YBCO disks. Utilising the inverse analysis algorithm presented in [22], the coefficients p_n were evaluated. A new undulator prototype was then assembled using the same disks, but sorted according to the distribution b_n proposed in this article, assuming $b_n \simeq p_n$. Finally, it was FCM at 10 T and its magnetic field profile measured during the entire charging phase. The full set of data is reported in Fig. 6, showing a clear improvement in field homogeneity. Fig. 7 provides a quantitative analysis of both prototypes, with the average undulator field B_0 and σ_B/B_0 among the central 17 peaks presented in the top and bottom sections of the plot, respectively. The σ_B was estimated with the following formula which rejects the impact of a non zero average of the peaks (B_i),

$$\sigma_B = \sqrt{\left(\sum_{i=1}^{N_1}(B_i^+ - B_0^+)^2 + \sum_{i=1}^{N_2}(B_i^- - B_0^-)^2\right)/N} \quad (11)$$

where B_i^+ are the positive peaks, B_0^+ is the mean value of the positive peaks, B_i^- are the negative peaks, B_0^- is the mean value of the negative peaks, N_1 is the number of positive peaks, and N_2 is the number of negative peaks ($N_1 = 8$, $N_2 = 9$, $N = N_1 + N_2 = 17$).

V. CONCLUSION AND OUTLOOK

The sorting algorithm proposed to minimise the undulator on-axis magnetic field errors was experimentally tested on a YBCO short prototype. The on-axis field homogeneity is significantly improved for the operating conditions, $B_s = 0$. The value of σ_B/B_0 drops from 23% before sorting to 7% after sorting; the mean undulator field B_0 slightly increases from 1.88 to 1.90 T within the expected statistical fluctuation. The achieved σ_B/B_0 reduction of a factor 3.2 validates the prediction (4±1.1) of the statistical model introduced in this article.

Extrapolating this result to our full scale prototype (200 bulks) indicates a potential improvement in the homogeneity of the on-axis undulator field by more than an order of magnitude, which substantiates the technical decision of a modular design made of independent disks. Additionally, by adjusting the heights of CoFe poles [23, 24], we expect that the field inhomogeneity can be further minimised and an RMS phase error [21] of only a few degrees can be achieved. Finally, cracks in the YBCO bulks were identified as the cause of the large initial spread among the undulator's poles, leading to a future systematic quality assessment of the YBCO bulks both before and after machining and embedding into the copper sleeves to prevent the assembly of faulty components.

VI. ACKNOWLEDGMENTS

[1] K. Halbach, Physical and optical properties of rare earth cobalt magnets, Nuclear Instruments and Methods in Physics Research **187**, 109 (1981).

[2] T. Hara, T. Tanaka, H. Kitamura, T. Bizen, X. Maréchal, T. Seike, T. Kohda, and Y. Matsuura, Cryogenic permanent magnet undulators, Phys. Rev. ST Accel. Beams **7**, 050702 (2004).

[3] M. Calvi, T. Schmidt, A. Anghel, A. Cervellino, S. J. Leake, P. R. Willmott, and T. Tanaka, Commissioning results of the U14 cryogenic undulator at sls, Journal of Physics: Conference Series **425**, 032017 (2013).

[4] Y. Ivanyushenkov, K. Harkay, M. Abliz, L. Boon, M. Borland, D. Capatina, J. Collins, G. Decker, R. Dejus, J. Dooling, C. Doose, L. Emery, J. Fuerst, J. Gagliano, Q. Hasse, M. Jaski, M. Kasa, S. H. Kim, R. Kustom, J. C. Lang, J. Liu, E. Moog, D. Robinson, V. Sajaev, K. Schroeder, N. Sereno, Y. Shiroyanagi, D. Skiadopoulos, M. Smith, X. Sun, E. Trakhtenberg, I. Vasserman,

A. Vella, A. Xiao, J. Xu, A. Zholents, E. Gluskin, V. Lev, N. Mezentsev, V. Syrovatin, V. Tsukanov, A. Makarov, J. Pfotenhauer, and D. Potratz, Development and operating experience of a short-period superconducting undulator at the advanced photon source, Phys. Rev. ST Accel. Beams **18**, 040703 (2015).

[5] S. Casalbuoni, A. Cecilia, S. Gerstl, N. Glamann, A. W. Grau, T. Holubek, C. Meuter, D. S. de Jauregui, R. Voutta, C. Boffo, T. Gerhard, M. Turenne, and W. Walter, Characterization and long term operation of a novel superconducting undulator with 15 mm period length in a synchrotron light source, Phys. Rev. Accel. Beams **19**, 110702 (2016).

[6] I. Asparuhov, *Staggered undulator X-ray source for low emittance electron storage ring*, Theses, Université Grenoble Alpes (2023).

[7] I. Kesgin, M. Kasa, Q. Hasse, Y. Ivanyushenkov, Y. Shiroyanagi, J. Fuerst, E. Barzi, D. Turrioni, A. V. Zlobin, and E. Gluskin, Development of short-period nb3sn superconducting planar undulators, IEEE Transactions on Applied Superconductivity **29**, 1 (2019).

[8] I. Kesgin, M. Kasa, Y. Ivanyushenkov, and U. Welp, High-temperature superconducting undulator magnets, Superconductor Science and Technology **30**, 04LT01 (2017).

[9] S. C. Richter, A. Ballarino, T. H. Nes, D. Schoerling, A. Bernhard, and A.-S. Müller, Status and powering test results of HTS undulator coils at 77 K for compact FEL designs, Journal of Physics: Conference Series **2420**, 012019 (2023).

[10] T. Tanaka, T. Hara, H. Kitamura, R. Tsuru, T. Bizen, X. Maréchal, and T. Seike, Application of high-temperature superconducting permanent magnets to synchrotron radiation sources, Phys. Rev. ST Accel. Beams **7**, 090704 (2004).

[11] T. Kii, H. Zen, N. Okawachi, M. Nakano, K. Masuda, H. Ohgaki, K. Yoshikawa, and T. Yamazaki, Design study on high-tc superconducting micro-undulator, in *Proceedings of FEL 2006, BESSY, Berlin, Germany* (2006).

[12] R. Kinjo, M. Shibata, T. Kii, H. Zen, K. Masuda, K. Nagasaki, and H. Ohgaki, Demonstration of a high-field short-period undulator using bulk high-temperature superconductor, Applied Physics Express **6**, 042701 (2013).

[13] J. H. Durrell, A. R. Dennis, J. Jaroszynski, M. D. Ainslie, K. G. B. Palmer, Y.-H. Shi, A. M. Campbell, J. Hull, M. Strasik, E. E. Hellstrom, and D. A. Cardwell, A trapped field of 17.6 T in melt-processed, bulk Gd-Ba-Cu-O reinforced with shrink-fit steel, Superconductor Science and Technology **27**, 082001 (2014).

[14] J. H. Durrell, M. D. Ainslie, D. Zhou, P. Vanderbemden, T. Bradshaw, S. Speller, M. Filipenko, and D. A. Cardwell, Bulk superconductors: a roadmap to applications, Superconductor Science and Technology **31**, 103501 (2018).

[15] M. Calvi, M. D. Ainslie, A. Dennis, J. H. Durrell, S. Hellmann, C. Kittel, D. A. Moseley, T. Schmidt, Y. Shi, and K. Zhang, A gdbco bulk staggered array undulator, Superconductor Science and Technology **33**, 014004 (2019).

[16] K. Zhang, A. Pirotta, X. Liang, S. Hellmann, M. Bartkowiak, T. Schmidt, A. Dennis, M. Ainslie, J. Durrell, and M. Calvi, Record field in a 10 mm-period bulk high-temperature superconducting undulator, Superconductor Science and Technology **36**, 05LT01 (2023).

[17] M. Calvi, S. Hellmann, E. Prat, T. Schmidt, K. Zhang, A. R. Dennis, J. H. Durrell, and M. D. Ainslie, Gdbco bulk superconducting helical undulator for x-ray free-electron lasers, Phys. Rev. Res. **5**, L032020 (2023).

[18] J. A. Clarke, *The Science and Technology of Undulators and Wigglers* (Oxford University Press, 2004).

[19] E. Prat, A. Al Haddad, C. Arrell, S. Augustin, M. Boll, C. Bostedt, M. Calvi, A. L. Cavalieri, P. Craievich, A. Dax, P. Dijkstal, E. Ferrari, R. Follath, R. Ganter, Z. Geng, N. Hiller, M. Huppert, R. Ischebeck, P. Juranić, C. Kittel, G. Knopp, A. Malyzhenkov, F. Marcellini, S. Neppl, S. Reiche, N. Sammut, T. Schietinger, T. Schmidt, K. Schnorr, A. Trisorio, C. Vicario, D. Voulot, G. Wang, and T. Weilbach, An x-ray free-electron laser with a highly configurable undulator and integrated chicanes for tailored pulse properties, Nature Communications **14**, 5069 (2023).

[20] C. Kittel, M. Calvi, S. Reiche, N. Sammut, G. Wang, and E. Prat, Enhanced X-ray free-electron laser performance with optical klystron and helical undulators, Journal of Synchrotron Radiation **31**, 948 (2024).

[21] R. Walker, Interference effects in undulator and wiggler radiation sources, Nuclear Instruments and Methods in Physics Research Section A: Accelerators, Spectrometers, Detectors and Associated Equipment **335**, 328 (1993).

[22] R. Kinjo, M. Calvi, K. Zhang, S. Hellmann, X. Liang, T. Schmidt, M. D. Ainslie, A. R. Dennis, and J. H. Durrell, Inverse analysis of critical current density in a bulk high-temperature superconducting undulator, Phys. Rev. Accel. Beams **25**, 043502 (2022).

[23] J. Pflüger, H. Lu, and T. Teichmann, Field fine tuning by pole height adjustment for the undulator of the TTF–FEL, Nuclear Instruments and Methods in Physics Research Section A: Accelerators, Spectrometers, Detectors and Associated Equipment **429**, 386 (1999).

[24] M. Calvi, C. Camenzuli, R. Ganter, N. Sammut, and T. Schmidt, Magnetic assessment and modelling of the Aramis undulator beamline, Journal of Synchrotron Radiation **25**, 686 (2018).